

New *N*-benzhydrylpiperazine/1,3,4-oxadiazoles conjugates inhibit the proliferation, migration, and induce apoptosis in HeLa cancer cells via oxidative stress-mediated mitochondrial pathway

Rashmin khanam¹  | Raj kumar² | Iram Iqbal Hejazi¹ | Syed Shahabuddin³ | Ramovatar Meena² | Paulraj Rajamani² | Nitin Yadav⁴ | Asif Iqbal Bhat⁵ | Fareeda Athar¹

¹Centre for Interdisciplinary Research in Basic Sciences, Jamia Millia Islamia, New Delhi, India

²School of Environmental Sciences, Jawaharlal Nehru University, New Delhi, India

³Research Centre for Nano-Materials and Energy Technology (RCNMET), School of Science and Technology, Sunway University, Selangor, Malaysia

⁴Department of Chemistry, Indian Institute of Technology, New Delhi, India

⁵Department of Chemistry, Sri Pratap College, Cluster University, Srinagar, India

Correspondence

Fareeda Athar, Centre for Interdisciplinary Research in Basic Sciences, Jamia Millia Islamia, Jamia Nagar, New Delhi 110025, India.
Email: fathar@jmi.ac.in

Funding information

University Grant Commission, IN, Grant/Award Number: (F.no-41-236/2012 (SR) and 13/07/2012

Abstract

N-benzhydrylpiperazine and 1,3,4-oxadiazoles are pharmacologically active scaffolds which exhibits significant inhibitory growth effects against various cancer cells, however, antiproliferation effects and the underlying mechanism for inducing apoptosis for aforementioned scaffolds addressing HeLa cancer cells remains uncertain. In this study, *N*-benzhydrylpiperazine clubbed with 1,3,4-oxadiazoles (**4a–4h**) were synthesized, subsequently characterized using high resolution spectroscopic techniques and eventually evaluated for their antiproliferation potential by inducing apoptosis in HeLa cancer cells. The MTT assay screening results revealed that among all, compound **4d** (*N*-benzhydryl-4-((5-(4-aminophenyl)-1,3,4-oxadiazol-2-yl)methyl)piperazine) in particular, exhibited IC₅₀ value of 28.13 ± 0.21 μg/mL and significantly inhibited the proliferation of HeLa cancer cells in concentration-dependent manner. The in vitro anticancer assays for treated HeLa cells resulted in alterations in the cell morphology, reduction in colony formation, and inhibition of cell migration in concentration-dependent treatment. Furthermore, G2/M phase arrest, variations in the nuclear morphology, degradation of chromosomal DNA confirmed the ongoing apoptosis in treated HeLa cells. Increase in the expression of cytochrome *C* and caspase-3 confirmed the involvement of intrinsic mitochondrial pathway regulating the cell death. Also, elevation in reactive oxygen species level and loss of mitochondrial membrane potential signified that compound **4d** induced apoptosis in HeLa cells by generating the oxidative stress. Therefore, compound **4d** may act as a potent chemotherapeutic agent against human cervical cancer.

KEYWORDS

antiproliferation, apoptosis, HeLa cancer cells, *N*-benzhydrylpiperazine/1,3,4-oxadiazoles conjugates, oxidative stress

1 | INTRODUCTION

Cervical cancer is one of the major causes of death among women worldwide. It is the fourth most frequently occurring cancer in women marked by 30% mortality rate within a period of 5 years of treatment.¹ Various external factors such as toxic chemicals, ionizing radiations, viruses, and certain internal factors mainly hormones, genetic mutations and weak immune conditions are involved in triggering or promoting the process of carcinogenesis.² In spite of various effective techniques available for treating cancer namely radiation therapy, chemotherapy, surgery, immunotherapy, cancer vaccinations, photo dynamic therapy, stem cell transformation,³ the mortality rate, and tendency for reoccurrence of cervical cancer among women still remains much higher in comparison with other types of cancers.⁴

Apoptosis is a programmed cell death regulating the systematic removal of dead, superfluous and damaged cells. It provides an effective mechanism for elimination of harmful cells besides playing a vital role in the maintenance and regulation of tissues homeostasis.^{5,6} Recent evidence had revealed that improper regulation of apoptosis promotes progress of carcinogenesis and ineffectiveness of drugs.⁷ Cellular processes like generation of reactive oxygen species (ROS) and loss of mitochondrial membrane potential are associated with the execution of the apoptosis pathways namely, extrinsic death receptor and intrinsic mitochondrial pathway.⁸ Treating cancer by inducing apoptosis through various chemotherapeutics is one the most fascinating approach in cancer research,⁹ however, many of these chemotherapeutic drugs lack efficiency due to the increased resistance.¹⁰ Thus, sequential apoptotic cell death and its role in facilitating various effective anticancer agents have drawn substantial attention.

There is drastic shift toward developing new synthetic compounds as potent chemotherapeutics. Based on the literature survey, *N*-benzhydrylpiperazine moiety emerged as one of the prominent heterocyclic scaffold exhibiting broad spectrum of biological activities such as antihistaminic,^{11,12} antimicrobial,¹³⁻¹⁵ antiviral.^{16,17} Recently, *N*-benzhydrylpiperazines has gained much popularity by displaying anticancer activities.¹⁸ Kumar et al¹⁹ had reported the cytotoxicity of *N*-benzhydrylpiperazine containing sulfonyl chlorides, acid chlorides, and isothiocyanates derivatives toward various cancer cells. Similarly, Yarim et al²⁰ had also reported anticancer activities of benzoyl chloride derivatives containing *N*-benzhydrylpiperazines toward liver, breast, colon, gastric, and endometrial cancer cell lines. The anticancer properties of piperazine nucleus is due to their abilities in inhibiting various growth factors, enzymes, and kinases, such as focal adhesion kinase (FAK),²¹ insulin-like growth

factor (IGF-1R),²² involve in regulation of cell death and generation of oxidative stress.²³ 1,3,4-Oxadiazoles, is another important scaffold demonstrating various pharmacological significances. The anticancer activities of 1,3,4-oxadiazole derivatives is contributed to their potential concerning the inhibition of telomerase,²⁴ histone deacetylase (HDAC),²⁵ thymidylate synthase (TS),²⁶ glyco-gen synthase kinase (GSK3),²⁷ vascular endothelial growth factor (VEGF),²⁸ and epidermal growth factor (EGFR)²⁹ involve in proliferation of cancer cells. Also, substitution at C-2 of 1,3,4-oxadiazoles by an acyl, or alkyl substrate further improves the biological profile.³⁰

Thus, taking into consideration the significant pharmacodynamics properties for both scaffolds, a new series of hybrids containing *N*-benzhydrylpiperazines and 1,3,4-oxadiazoles moieties have been synthesized (Figure 1) with an objective to explore their resonating antiproliferative properties and to investigate the possible molecular mechanism involved in induction of apoptosis in cervical cancer cell line (HeLa).

2 | MATERIALS AND METHODS

2.1 | Chemistry

Reagents used in synthesis were purchased commercially and used without any further purification. Column chromatography was performed using silica gel (200 mesh) brought from Sigma Aldrich (India). The purity of compounds was evaluated using CHN Elemental analyzer (Vario EL-III; Elementar Analysensysteme GmbH, Dnaustrasse, Hanau, Germany) and experimental values were found within the range of $\pm 0.3\%$ with that of calculated values. Melting points for all compounds were determined using MEL-temp

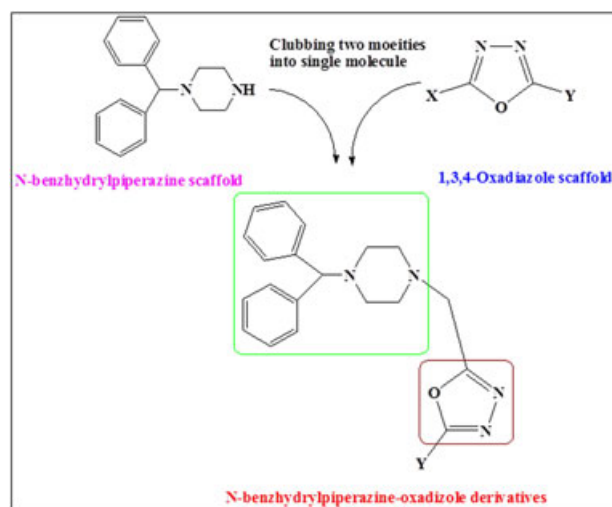


FIGURE 1 General structure of derivatives containing *N*-Benzhydrylpiperazine and 1,3,4-oxadiazoles

apparatus and all values were uncorrected. Bruker Tensor 37 Fourier-transform infrared (FT-IR) spectrometer (Selangor, Malaysia) was used to obtain IR spectra for all compounds. The $^1\text{H-NMR}$ and $^{13}\text{C-NMR}$ spectra were obtained using $\text{CDCl}_3/\text{DMSO-d}_6$ as solvents on Bruker Advance spectrometer (Selangor, Malaysia) at 300 MHz. AB-Sciex 2000 instrument (Ontario, Canada) was used to obtain the electrospray ionization-mass spectra (ESI-MS).

2.1.1 | General procedure for synthesis of *N*-benzhydrylpiperazines-1,3, 4-oxadiazole hybrids (4a–4h)

A volume of 5 mL of phosphorous oxychloride was added dropwise to the solution containing intermediate (3) (1 mmol) and substituted benzoic acid (1 mmol) and was kept for refluxing for about 12 to 15 hours. On completion, reaction mixture was cooled to the room temperature and poured over crushed ice followed by neutralization using 5% sodium bicarbonate solution. Precipitates so obtained were filtered and dried. Crude product was then further purified through recrystallization using a solvent mixture (dichloromethane:methanol, 1:1).

N-benzhydryl-4-((5-phenyl)-1,3, 4-oxadiazol-2-yl) methylpiperazine (4a)

Yield: 51.6%; mp: 153 to 155°C; Anal Calcd for $\text{C}_{26}\text{H}_{26}\text{N}_4\text{O}$: C, 76.07; H, 6.38; N, 13.65; found C, 76.06; H, 6.38; N, 13.63; IR (ν_{max} cm^{-1}): 3276 (NH stretch), 3100, 3000 (Ar-H) 2941, 2827 (piperazine ring), 1620, 1463 (C=N, C=C), 1252, 1045 (C–O–C), 1380 (C–N)¹; $^1\text{H-NMR}$ (DMSO-d_6) δ (ppm): 7.42 to 7.40 (d, 4H, Ar-H, $J = 6.6$ Hz), 7.31 to 7.29 (t, 4H, Ar-H, $J = 6.7$ Hz), 7.24 to 7.20 (m, 5H, phenyl), 7.19 to 7.17 (d, 2H, Ar-H, $J = 6.6$ Hz), 4.94 (s, 2H, $-\text{CH}_2$), 4.29 (s, 1H, $-\text{CH}$), 3.2 (br, s, 4H, $-\text{CH}_2\text{-N-CH}_2$, piperazine ring), 2.35 (br, s, 4H, $-\text{CH}_2\text{-N-CH}_2$, piperazine ring) $^{13}\text{C-NMR}$ (DMSO-d_6) δ (ppm) 176.35, 168.5, 152.67, 145.45, 137.45, 135.34, 133.76, 128.88, 127.3, 126.7, 122.2, 119.68, 116.11, 70.3, 59.1, 49.75, 45.31; ESI-MS m/z : $[\text{M}+\text{H}]^+$ 411.2.

N-benzhydryl-4-((5-(2-chlorophenyl)-1,3,4-oxadiazol-2-yl)methyl)piperazine (4b)

Yield: 46.46%; mp: 161 to 163°C; Anal Calcd for $\text{C}_{26}\text{H}_{25}\text{ClN}_4\text{O}$: C, 70.18; H, 5.66; N, 12.59; found C, 70.16; H, 5.68; N, 12.59; IR (ν_{max} cm^{-1}): 3216 (NH stretch), 3101, 3016 (Ar-H), 2943, 2817 (piperazine ring), 1618, 1458 (C=N, C=C), 1256, 1123 (C–O–C), 1293 (C–N); $^1\text{H-NMR}$ (CDCl_3) δ (ppm): 7.39 to 7.37 (d, 4H, Ar-H, $J = 6.6$ Hz), 7.33 to 7.31 (t, 4H, Ar-H, $J = 6.7$ Hz), 7.25 to 7.21 (m, 5H, phenyl), 7.16 to 7.15 (d, 2H, Ar-H, $J = 6.6$ Hz), 4.91 (s, 2H, $-\text{CH}_2$), 4.31 (s, 1H, $-\text{CH}$), 3.19 (br, s, 4H, $-\text{CH}_2\text{-N-CH}_2$, piperazine ring), 2.33 (br, s, 4H, $-\text{CH}_2\text{-N-CH}_2$, piperazine

ring) $^{13}\text{C-NMR}$ (CDCl_3) δ (ppm) 171.55, 164.15, 151.77, 143.65, 139.65, 136.34, 135.26, 129.18, 128.3, 127.7, 121.2, 117.38, 115.84, 73.4, 56.2, 48.35, 45.01; ESI-MS m/z : $[\text{M} + 2]$ 446.96.

N-benzhydryl-4-((5-(2,4-dichlorophenyl)-1,3, 4-oxadiazol-2-yl)methyl)piperazine (4c)

Yield: 43.76%; mp: 165 to 167°C; Anal Calcd for $\text{C}_{26}\text{H}_{24}\text{Cl}_2\text{N}_4\text{O}$: C, 65.14, H, 5.05, N, 11.69; found C, 65.16, H, 5.06, N, 11.69; IR (ν_{max} cm^{-1}): 3200 (NH stretch), 3107, 3067 (Ar-H), 2914, 2800 (piperazine ring), 1613, 1446 (C=N, C=C), 1243, 1119 (C–O–C), 1291 (C–N); $^1\text{H-NMR}$ (CDCl_3) δ (ppm): 7.35 to 7.33 (d, 4H, Ar-H, $J = 6.6$ Hz), 7.30 to 7.29 (t, 4H, Ar-H, $J = 6.7$ Hz), 7.21 to 7.19 (m, 5H, phenyl), 7.14 to 7.13 (d, 2H, Ar-H, $J = 6.6$ Hz), 4.88 (s, 2H, $-\text{CH}_2$), 4.29 (s, 1H, $-\text{CH}$), 3.23 (br, s, 4H, $-\text{CH}_2\text{-N-CH}_2$, piperazine ring), 2.43 (br, s, 4H, $-\text{CH}_2\text{-N-CH}_2$, piperazine ring) $^{13}\text{C-NMR}$ (CDCl_3) δ (ppm) 173.15, 163.75, 153.37, 145.45, 138.35, 134.04, 132.36, 129.58, 128.23, 126.47, 120.22, 116.18, 113.64, 70.94, 66.82, 45.65, 43.81; ESI-MS m/z : $[\text{M} + 2]$ 481.4.

N-benzhydryl-4-((5-(4-aminophenyl)-1,3, 4-oxadiazol-2-yl)methyl)piperazine (4d)

Yield: 49.46%; mp: 146 to 148°C; Anal Calcd for $\text{C}_{26}\text{H}_{27}\text{N}_5\text{O}$: C, 73.39, H, 6.40, N, 16.46; found C, 73.40, H, 6.41, N, 16.45; IR (ν_{max} cm^{-1}): 3201 (NH stretch), 3116, 3058 (Ar-H), 2954, 2832 (piperazine ring), 1623, 1470 (C=N, C=C), 1239, 1123 (C–O–C), 1265 (C–N) $^1\text{H-NMR}$ (CDCl_3) δ (ppm): 7.74 to 7.72 (d, 4H, Ar-H, $J = 6.6$ Hz), 7.26 to 7.23 (t, 4H, Ar-H, $J = 6.7$ Hz), 6.97 to 6.94 (m, 5H, phenyl), 6.92 to 6.91 (d, 2H, Ar-H, $J = 6.6$ Hz), 5.33 (s, 2H, $-\text{NH}_2$), 4.67 (s, 2H, $-\text{CH}_2$), 4.13 (s, 1H, $-\text{CH}$), 3.10 (br, s, 4H, $-\text{CH}_2\text{-N-CH}_2$, piperazine ring), 2.50 (br, s, 4H, $-\text{CH}_2\text{-N-CH}_2$, piperazine ring) $^{13}\text{C-NMR}$ (CDCl_3) δ (ppm) 177.31, 167.63, 151.62, 141.45, 134.59, 131.51, 130.96, 129.43, 128.83, 127.62, 115.30, 114.51, 77.52, 62.34, 60.72, 40.85, 40.61; ESI-MS m/z : $[\text{M} + \text{H}]^+$ 426.53.

N-benzhydryl-4-((5-(4-methylphenyl)-1,3, 4-oxadiazol-2-yl)methyl)piperazine (4e)

Yield: 51.06%; mp: 143 to 145°C; Anal Calcd for $\text{C}_{27}\text{H}_{28}\text{N}_4\text{O}$: C, 76.39, H, 6.65, N, 13.20; found C, 76.40, H, 6.64, N, 13.21; IR (ν_{max} cm^{-1}): 3301 (NH stretch), 3289, 3123 (Ar-H), 2900, 2885 (piperazine ring), 1618, 1458 (C=N, C=C), 1242, 1117 (C–O–C), 1263 (C–N); $^1\text{H-NMR}$ (DMSO-d_6) δ (ppm): 7.38 to 7.37 (d, 4H, Ar-H, $J = 6.6$ Hz), 7.33 to 7.31 (t, 4H, Ar-H, $J = 6.7$ Hz), 7.24 to 7.19 (m, 5H, phenyl), 7.13 to 7.12 (d, 2H, Ar-H, $J = 6.6$ Hz), 4.81 (s, 2H, $-\text{CH}_2$), 4.47 (s, 1H, $-\text{CH}$), 3.23 (br, s, 4H, $-\text{CH}_2\text{-N-CH}_2$, piperazine ring), 2.46 (br, s, 4H, $-\text{CH}_2\text{-N-CH}_2$, piperazine ring) $^{13}\text{C-NMR}$ (DMSO-d_6) δ (ppm) 172.25, 164.53, 151.52, 143.52, 134.45, 132.11,

129.36, 127.48, 126.73, 122.28, 117.12, 114.21, 112.45, 67.94, 64.32, 45.85, 41.31; ESI-MS m/z : $[M + H]^+$ 425.54.

***N*-benzhydryl-4-((5-(4-tertbutylphenyl)-1,3,4-oxadiazol-2-yl)methyl)piperazine (4f)**

Yield: 47.34%; mp: 161 to 163°C; Anal Calcd for $C_{30}H_{34}N_4O$: C, 77.22, H, 7.34, N, 12.01; found C, 77.21, H, 7.33, N, 12.02; IR (ν_{\max} cm^{-1}): 3388 (NH stretch), 3206, 3101 (Ar-H), 2900, 2865 (piperazine ring), 1623, 1515 (C=N, C=C), 1276, 1106 (C-O-C), 1253 (C-N); 1H -NMR ($CDCl_3$) δ (ppm): 7.32 to 7.31 (d, 4H, Ar-H, $J = 6.6$ Hz), 7.28 to 7.26 (t, 4H, Ar-H, $J = 6.7$ Hz), 7.20 to 7.15 (m, 5H, phenyl), 7.10 to 7.09 (d, 2H, Ar-H, $J = 6.6$ Hz), 4.76 (s, 2H, $-CH_2$), 4.47 (s, 1H, $-CH$), 3.19 (br, s, 4H, $-CH_2-N-CH_2$, piperazine ring), 2.44 (br, s, 4H, $-CH_2-N-CH_2$, piperazine ring) ^{13}C -NMR (DMSO- d_6) δ (ppm) 170.56, 165.30, 153.67, 141.82, 135.75, 132.11, 130.96, 128.98, 127.03, 123.18, 116.82, 113.82, 111.56, 65.74, 63.72, 44.09, 40.90; ESI-MS m/z : $[M + H]^+$ 467.62.

***N*-benzhydryl-4-((5-(2-nitrophenyl)-1,3,4-oxadiazol-2-yl)methyl)piperazine (4g)**

Yield: 38.12%; mp: 173 to 175°C; Anal Calcd for $C_{26}H_{25}N_5O_3$: C, 68.56, H, 5.53, N, 15.37; found C, 68.55, H, 5.54, N, 15.38; IR (ν_{\max} cm^{-1}): 3309 (NH stretch), 3275, 3112 (Ar-H), 2900, 2812 (piperazine ring), 1626, 1523 (C=N, C=C), 1246, 1123 (C-O-C), 1234 (C-N) 1H -NMR ($CDCl_3$) δ (ppm): 7.36 to 7.35 (d, 4H, Ar-H, $J = 6.6$ Hz), 7.26 to 7.24 (t, 4H, Ar-H, $J = 6.7$ Hz), 7.15 to 7.10 (m, 5H, phenyl), 7.12 to 7.11 (d, 2H, Ar-H, $J = 6.6$ Hz), 4.86 (s, 2H, $-CH_2$), 4.56 (s, 1H, $-CH$), 3.46 (br, s, 4H, $-CH_2-N-CH_2$, piperazine ring), 2.83 (br, s, 4H, $-CH_2-N-CH_2$, piperazine ring) ^{13}C -NMR ($CDCl_3$) δ (ppm) 172.40, 163.32, 152.87, 140.45, 134.23, 132.46, 129.32, 128.12, 123.31, 121.32, 115.21, 114.23, 112.98, 64.10, 62.39, 42.13, 41.45; ESI-MS m/z : $[M + H]^+$ 456.51.

***N*-benzhydryl-4-((5-(4-nitrophenyl)-1,3,4-oxadiazol-2-yl)methyl)piperazine (4h)**

Yield: 43.62%; mp: 183 to 185°C; Anal Calcd for $C_{26}H_{25}N_5O_3$: C, 68.56, H, 5.53, N, 15.37; found C, 68.55, H, 5.54, N, 15.38; IR (ν_{\max} cm^{-1}): 3321 (NH stretch), 3254, 3109 (Ar-H), 2976, 2843 (piperazine ring), 1634, 1521 (C=N, C=C), 1242, 1134 (C-O-C), 1256 (C-N) 1H -NMR (DMSO- d_6) δ (ppm): 7.67 to 7.65 (d, 4H, Ar-H, $J = 6.6$ Hz), 7.63 to 7.61 (t, 4H, Ar-H, $J = 6.7$ Hz), 7.59 to 7.53 (m, 5H, phenyl), 7.51 to 7.50 (d, 2H, Ar-H, $J = 6.6$ Hz), 4.81 (s, 2H, $-CH_2$), 4.47 (s, 1H, $-CH$), 3.56 (br, s, 4H, $-CH_2-N-CH_2$, piperazine ring), 2.80 (br, s, 4H, $-CH_2-N-CH_2$, piperazine ring) ^{13}C -NMR (DMSO- d_6) δ (ppm) 171.25, 164.62, 154.40, 141.32, 133.33, 131.52, 130.74, 128.42, 127.86, 122.10, 113.19, 112.71, 62.34, 60.71, 40.32, 40.06, 39.76, 39.48. ESI-MS m/z : $[M + H]^+$ 456.51.

2.2 | Pharmacology

2.2.1 | Antibodies and reagents

Media RPMI-1640, fetal bovine serum (FBS), and trypsin were purchased from GIBCO Grand Island (New York, NY) whereas all the important reagents were purchased from Sigma Aldrich (St Louis, MO). Primary mice β -actin, primary rabbit cytochrome *C* (cyt *C*), primary mice caspase-3 and secondary antimice @@@immunoglobulin G-horseradish peroxidase (IgG-HRP) and antirabbit IgG-HRP antibodies were brought from Santa Cruz Biotechnology (Santa Cruz, TX). All other chemicals used were of molecular biology grade.

2.2.2 | Cell culture

HeLa (human cervical cancer cell line) was bought from National Centre for Cell Science, Department of Biotechnology (Pune, India). Cells were incubated at 37°C in RPMI-1640 medium as monolayer supplemented with 10% (vol/vol) FBS and antibiotics (penicillin 100 U/mL and streptomycin 10 μ g/mL) and 1 mmol/L sodium pyruvate.

2.2.3 | Cell proliferation (MTT assay)

Cells with density of 5×10^3 cells per well were seeded in 96-well plate and kept overnight. Media was changed and cells were treated with synthesized compounds (**4a-4h**) (12.5 to 100 μ g/mL) for 24 hours followed by addition of 20 μ L containing 5 mg/mL of MTT to each well 4 hours before completion of incubation. The percentage of inhibition was calculated using following formula:³¹

Percent inhibition

$$= \frac{\text{Mean OD of untreated cells (control)} - \text{Mean OD of treated cells}}{\text{Mean OD of untreated cells (control)}} \times 100,$$

while the IC_{50} values for all compounds were obtained by plotting curves between percentage of inhibition and concentration of derivatives.

2.2.4 | Morphological changes of treated HeLa cells

A total of 1×10^3 cells were seeded in 60 mm plates followed by treatment with compound (**4d**). Nikon microscope (ECLIPSE Ti-S, Tokyo, Japan) was used to study the morphology of cells after 24 hours.

2.2.5 | In vitro clonogenic assay

A total of 1×10^3 cells per well were seeded on six-well plates, followed by incubation at 37°C. Media was replaced

twice; cells were washed thoroughly twice with phosphate-buffered saline (PBS), fixed for 10 minutes, stained with crystal violet solution and noticed through naked eyes.

2.2.6 | In vitro cell migration assay

A total of 1×10^3 cells per well was seeded equally in six-well plates, when cells growth reached 80% confluence; a scratch was made using 200 μ L pipette tip containing compound **4d**. The photographs of cell scratch were taken at 0 hour and 24 hours using Nikon microscope (ECLIPSE Ti-S) and percentage of wound thickness was measured by the ratio of wound thickness after 24 hours to 0 hour

2.2.7 | Cell cycle analysis

The cell cycle analysis was carried out according to the reported protocol.³² The HeLa cells seeded in 60 mm dish and treated with compound **4d** for 24 hours. The fluorescence displayed by each Pi-DNA complex containing 20 000 cells was used to quantify the apoptotic cells with the help of FACS Caliber instrument (Becton Dickinson, Franklin Lakes, NY).

2.2.8 | Acridine orange and ethidium bromide dual fluorescent assay

The acridine orange (AO) and ethidium bromide (EtBr) dual staining assay was used to evaluate the apoptosis in HeLa cells. Cells were suspended in a mixture containing EtBr/AO dual staining solution in the 1:1 ratio in PBS for 2 minutes. Stained cells were observed through Nikon fluorescence microscope (ECLIPSE Ti-E).

2.2.9 | DNA fragmentation assay

Cells were treated with compound **4d** for 24 hours. Spectrophotometer Nano Drop (Nano Drop, Wilmington, DE) was used to quantify DNA extract. Two percent of agarose gel along with 1 μ g/1 mL EtBr was taken to electrophoresis the DNA samples. The gel was studied and images were taken using ultraviolet gel documentation.

2.2.10 | Measurement of cellular ROS

Cells in density of 5×10^5 cells per well were seeded over the cover slip of six-plated well and left for incubation to attain attachment. The following day, cells were suspended in fresh media containing compound **4d**. Cells were incubated for 4 hours at 37°C and stained using 40 μ M of dichloro-dihydro-fluorescein diacetate (DCFHDA) dye for

30 minutes. Images were observed using fluorescence microscope (Nikon ECLIPSE Ti-E).

2.2.11 | Evaluation of mitochondrial membrane potential (ψ_m)

The loss of ψ_m was evaluated using mitochondrial-membrane-permeable JC-1 dye. Six-well plate was used to seed cells having density of 1×10^3 cells per well followed by treatment with compound **4d**. After 4 hours treatment, cells were washed using PBS, stained with 2 μ g/mL of JC-1 and kept for incubation at 37°C for 30 minutes. Live imaging microscope was used for capturing images. Mitochondrial-membrane potential was evaluated with the help of fluorimeter after cells were treated with compound **4d**. After cells being incubated at 37°C for 4 hours, cells were stained using JC-1 (10 μ g/mL in PBS) dye at 37°C. Finally, cells were harvested and washed with saline phosphate buffer and results were taken at 530 and 590 nm.

2.2.12 | Protein extraction and Western blot analysis

Cells were equally seeded in 100 mm plate, after 80% confluence, cells were treated for 24 hours with compound **4d**. After that, cells were trypsinized and washed using PBS. Extraction of protein and estimation of protein concentration was done using Radio Immuno Precipitation Assay (RIPA) buffer, respectively. The protein was separated in 8% sodium dodecyl sulfate polyacrylamide gel electrophoresis (SDS-PAGE) gel and moved to nitrocellulose membrane. Membrane was obstructed using 5% bovine serum albumin in PBS. After that it was probed with primary antibody and incubated with secondary antibody conjugate using HRP. The bands were detected using ECL kit and images were captured permanently as X-ray films. Results were observed with reference to the loading control (β -actin).

2.2.13 | Estimation of cytosolic cyt C

Measurement of the protein concentration in cytosolic fraction was done using Bradford dye (Sigma Aldrich, India) according to the reported protocol.³² The extracted protein was taken in 8% SDS-PAGE gel for Western blot analysis.

2.2.14 | Data interpretation

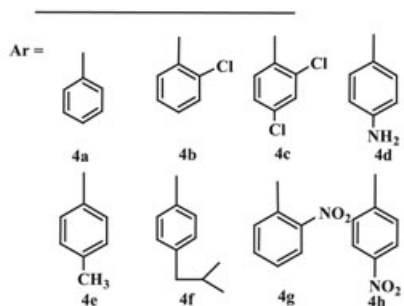
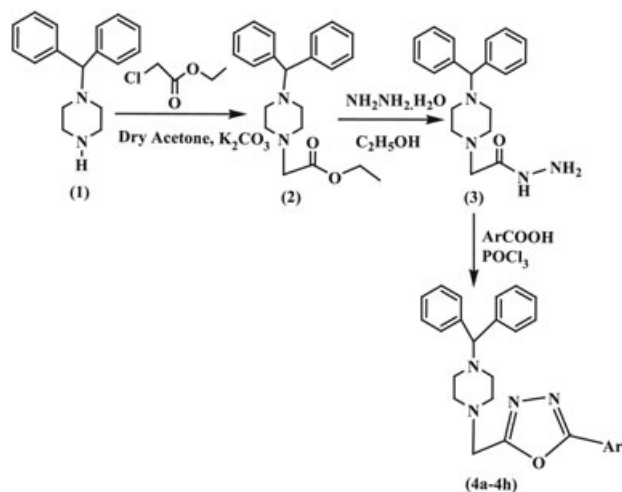
All the experimental data was taken as mean \pm SD for set of three independent experiments. The value of significance (*P* values) was estimated using unpaired Student *t* test of the Graph Pad Prism Version 7.0 (Jamia Millia

Islamia, New Delhi, India) software. *P* value of less than 0.05 is considered to be statistically significant.

3 | RESULTS

3.1 | Chemistry

N-benzhydrylpiperazine/1,3,4-oxadiazoles conjugates (**4a-4h**) were synthesized according to the chemical reactions as presented in Scheme 1. Formation of ethyl-2-(4-benzhydrylpiperazin-1-yl) acetate (**2**) and 2-(4-benzhydrylpiperazin-1-yl) acetohydrazide (**3**), the prime intermediates involved in synthesis of target compounds (**4a-4h**) were prepared according to the reported protocol.³³ The final derivatives (**4a-4h**) were synthesized through cyclization of main intermediate (**3**) by refluxing it with different carboxylic acid derivatives in POCl₃. Spectroscopic data so obtained from FT-IR, Proton/C-NMR, ESI-MS, and CHN analysis confirmed the synthesis of desired compounds. The final derivatives (**4a-4h**) showed presence of new absorption bands at 3261, 1600, 1316, and 1160 cm⁻¹ corresponding to amido (-NH), imine (C=N) and -C-O-C functional groups, respectively confirming the cyclization of intermediate (**3**). ¹H-NMR spectra further confirmed the



SCHEME 1 *N*-benzhydrylpiperazine/1,3,4-oxadiazoles derivatives (**4a-4h**)

formation of desired products (**4a-4h**) through appearance of addition peaks in range of δ 7.25 to 7.20 representing aromatic protons. Also, ¹³C-NMR spectra confirmed the formation of final products (**4a-4h**) through appearance of new peaks at δ 176.36 and 168.98 representing C-2 and C-5 carbon atoms of 1,3,4-oxadiazole ring, respectively. While the peaks in range of δ 122.34 to 137.68 represented the phenyl ring (Supporting Information Figures S2-S5). Further, the synthesis of final compounds (**4a-4h**) was confirmed through ESI-MS.

3.2 | Pharmacology

3.2.1 | Cell growth inhibition assay

MTT assay was used to study the plausible effects of *N*-benzhydrylpiperazine/1,3,4-oxadiazoles conjugates (**4a-4h**) on the proliferation and survival of HeLa cells. The cells were treated with final derivatives (**4a-4h**) along with the standard anticancer drug “5-Fluorouracil” in the concentration range of 12.5 to 100 μ g/mL for 24 hours (Table 1). Among all, compound **4d** in particular, significantly inhibited the growth of HeLa cancer cells with IC₅₀ value 28.13 \pm 0.21 μ g/mL which was considerably higher than the standard drug 5-fluorouracil (IC₅₀ value of 111.45 \pm 0.03 μ g/mL). Besides that, compound **4** hours also moderately inhibited the growth of HeLa cells with IC₅₀ 35.97 \pm 1.22 μ g/mL while all other derivatives displayed no inhibitory effects up till 100 μ g/mL concentrations (Supporting information Figure S1).

3.2.2 | Assessment of molecular properties of synthesized compounds

Based on the Lipinski rule of five, all the final derivatives (**4a-4h**) were analyzed for some molecular properties which are physically and pharmaceutically important. All the derivatives exhibited optimum drug likeness properties and showed no violations from the Lipinski rule of five (Table 2).³⁴

3.2.3 | Cell proliferation and colony formation inhibited by *N*-benzhydryl-4-((5-(4-aminophenyl)-1,3,4-oxadiazol-2-yl)methyl)piperazine (**4d**)

Based on the MTT screening results, the compound **4d** considerably inhibited the proliferation of HeLa cancer cells. Further treating the HeLa cells with compound **4d** in different concentrations induced some of the cell morphological changes such as cell shrinkage, spike formation, and appearance of dead cells as observed through microscope

TABLE 1 Antiproliferative activity of *N*-benzhydrylpiperazine containing 1,3,4-oxadiazole derivatives (**4a-4h**)

Compound No.	Ar group	HeLa ¹ IC ₅₀ (μg/ml)±S.D
4a.		>100
4b.		>100
4c.		>100
4d.		28.13±0.2
4e.		>100
4f.		>100
4g.		>100
4h.		35.97±1.22
5-Fluorouracil²	-	111.45±0.03

No activity >100 μM; Bold values represent active compounds.

The values (in μg/mL) represent the mean ± SE of three independent experiments.

IC₅₀ is the concentration required to inhibit 50% of the cell population.

Standard drug was used for reference. HeLa: human cervical cancer cell line.

TABLE 2 Molecular properties of compounds

Compound no	Mi Log <i>P</i>	TPSA	MW	<i>n</i> ON	<i>n</i> OHNH	<i>n</i> rotb		
Desirable value	<5	<140	natoms	<500	<10	<5	Volume	<10
4a	4.23	45.40	31	410.52	5	0	387.09	6
4b	4.86	45.40	32	444.97	5	0	400.6	6
4c	5.52	45.40	33	479.41	5	0	414.16	6
4d	3.31	71.42	32	425.54	6	2	398.38	6
4e	4.68	45.40	32	424.55	5	0	403.65	6
4f	5.53	45.40	35	466.63	5	0	453.84	8
4g	4.14	91.22	34	455.52	8	0	410.42	7
4h	4.19	91.22	34	455.52	8	0	410.42	7

Abbreviations: MW, molecular weight; natoms, number of atoms; *n*ON, number of hydrogen bond acceptors; *n*OHNH, number of hydrogen bond donors; *n*rotb, number of rotatable bonds; Mi Log *P*, Log *P* value predicted by molinspiration; TPSA, topological polar surface area.

(Figure 2A). Also, to evaluate the unanchored growth ability of each cell, clonogenic assay was performed. As shown in figure, the size and number of colonies of HeLa cells decreased remarkably in the concentration dependent treatment with compound **4d** (Figure 2B). Thus, it was clearly suggested that compound **4d** induced morphological changes and inhibited proliferation of HeLa cells in comparison with control cells (untreated cells) which were intact, normal shaped, and proliferated to form colonies.

3.2.4 | *N*-benzhydryl-4-((5-(4-aminophenyl)-1,3,4-oxadiazol-2-yl)methyl)piperazine (**4d**) inhibited the cell migration

In addition to above experiments, we also carried out in vitro wound healing assay to investigate the migratory potential of treated HeLa cells. As shown in (Figure 3A), the thickness of wound increased largely in HeLa cells treated in a concentration dependent manner due to inhibition of cell

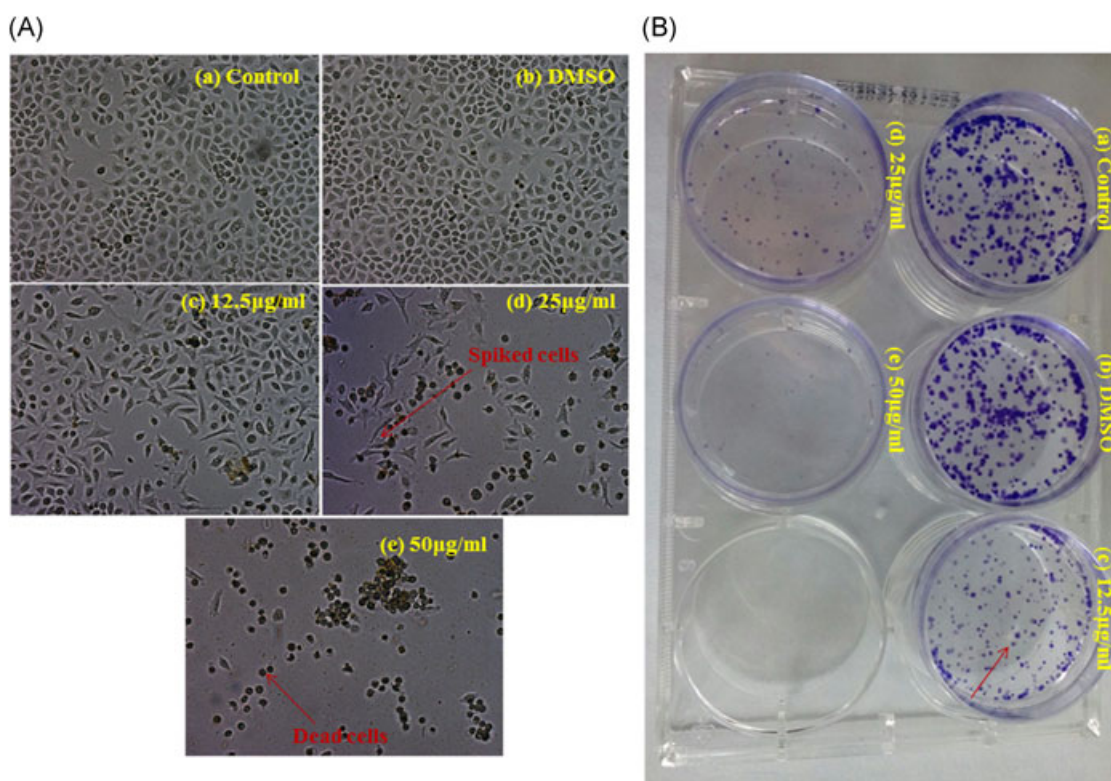


FIGURE 2 Effect of different concentrations of **4d** compound on HeLa cells after 24 hours treatment. A, Morphological changes such as spikes formation and dead cells were observed. (Images were captured using Nikon inverted ECLIPSE Ti-S microscope at $\times 10$ magnification). B, Clonogenic assay (crystal violet staining). Arrow shows that the size and numbers of colonies were reduced. DMSO, dimethyl sulfoxide

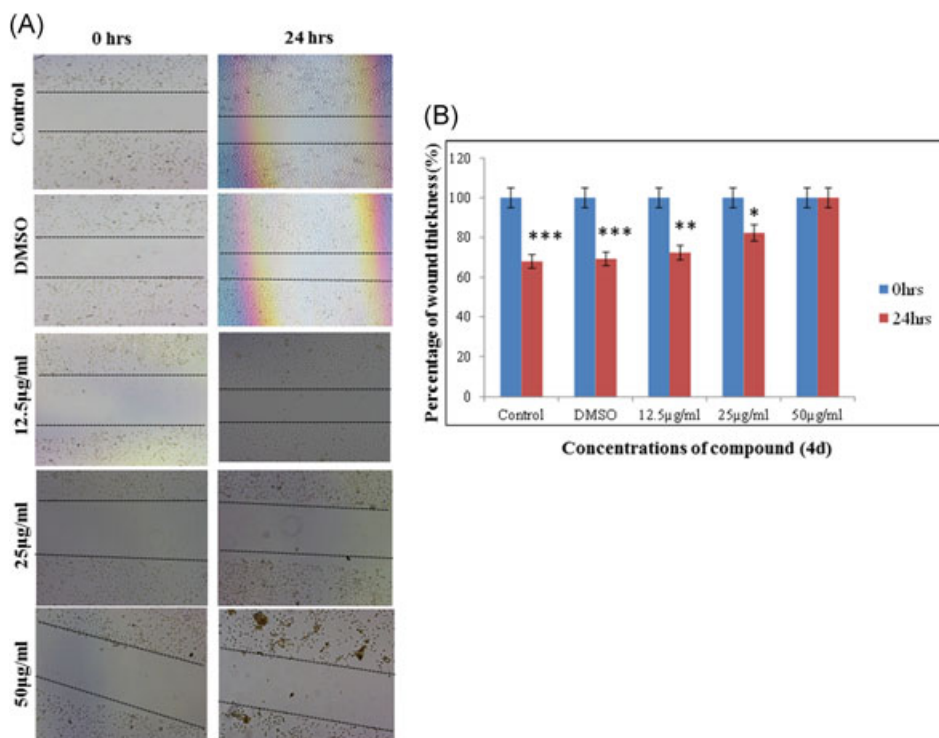


FIGURE 3 A, Effect of different concentrations of compound **4d** on in vitro migration potential of HeLa cells at 0 and 24 hours. Scratches were created with sterile 200 mL pipette and images were captured using microscope (Nikon ECLIPSE Ti-S). B, Bar graph representing the relative percentage of wound thickness for different concentrations of compound **4d** at 0 and 24 hours. Data are mean \pm SD from three independent experiments, each with triplicates. *** $P < 0.0001$, ** $P < 0.01$, and * $P < 0.1$ significant vs control. DMSO, dimethyl sulfoxide

migration induced by compound **4d** whereas for untreated cells control the thickness of wound decreased due to migratory potential of cancer cells. Increase in the percentage of wound thickness was also observed for compound **4d** from 67.94% (control) to 69.23% (DMSO), 72.32% (12.5 $\mu\text{g/mL}$), 82.35% (25 $\mu\text{g/mL}$), and 96.15% (50 $\mu\text{g/mL}$) concentrations respectively (Figure 3B). The data clearly suggested that compound **4d** substantially inhibited the cell migration.

3.2.5 | *N*-benzhydryl-4-((5-(4-aminophenyl)-1,3,4-oxadiazol-2-yl)methyl)piperazine (**4d**) induced an arrest in G2/M phase of cell cycle and apoptosis in HeLa cells

Flow cytometry was used to analyze the distribution and proportion of apoptotic cells in different phases of cell cycle. HeLa cells after being treated with compound **4d** for 24 hours, displayed considerable increase in the population of cells in G2/M phase ($P < 0.05$) from 16.74% (control) to 17.90% (DMSO), 19.84%, 23.03%, and 28.97% at 12.5, 25, and 50 $\mu\text{g/mL}$ concentrations of compound **4d**, respectively (Figure 4A) with simultaneous decrease in the ratio of HeLa cells in sub-G1 phase ($P < 0.05$) (Figure 4B).

These results clearly showed that compound **4d** inhibited the proliferation of HeLa cells by inducing cell cycle arrest at G2/M phase.

To further investigate the apoptotic inducing abilities of compound **4d**, we evaluated the variations in nuclear morphology and fragmentation of chromosomal DNA. The cell death induced by compound **4d** in HeLa cells is associated with certain characteristic morphological changes, which were evaluated by treating HeLa cells with AO/EtBr stains in concentration dependent manner and observed under fluorescence microscope. As shown in Figure 4C, live cells appeared uniformly green having intact membrane and uniform chromatin, whereas early apoptotic cells and late apoptotic cells appeared as bright green and orange, respectively, signifying the chromatin condensation and nuclear fragmentation. Conversely, necrotic cells appeared red with no condensed chromatin.

Further, fragmentation of chromosomal DNA was studied using agarose gel electrophoresis. Chromosomal DNA treated with compound **4d** displayed a ladder like pattern of DNA fragments comprising multiples of roughly 180 to 200 base pairs while the untreated cells showed intact bands (Figure 4D). All these data collectively indicated that compound **4d** caused apoptosis in HeLa cells.

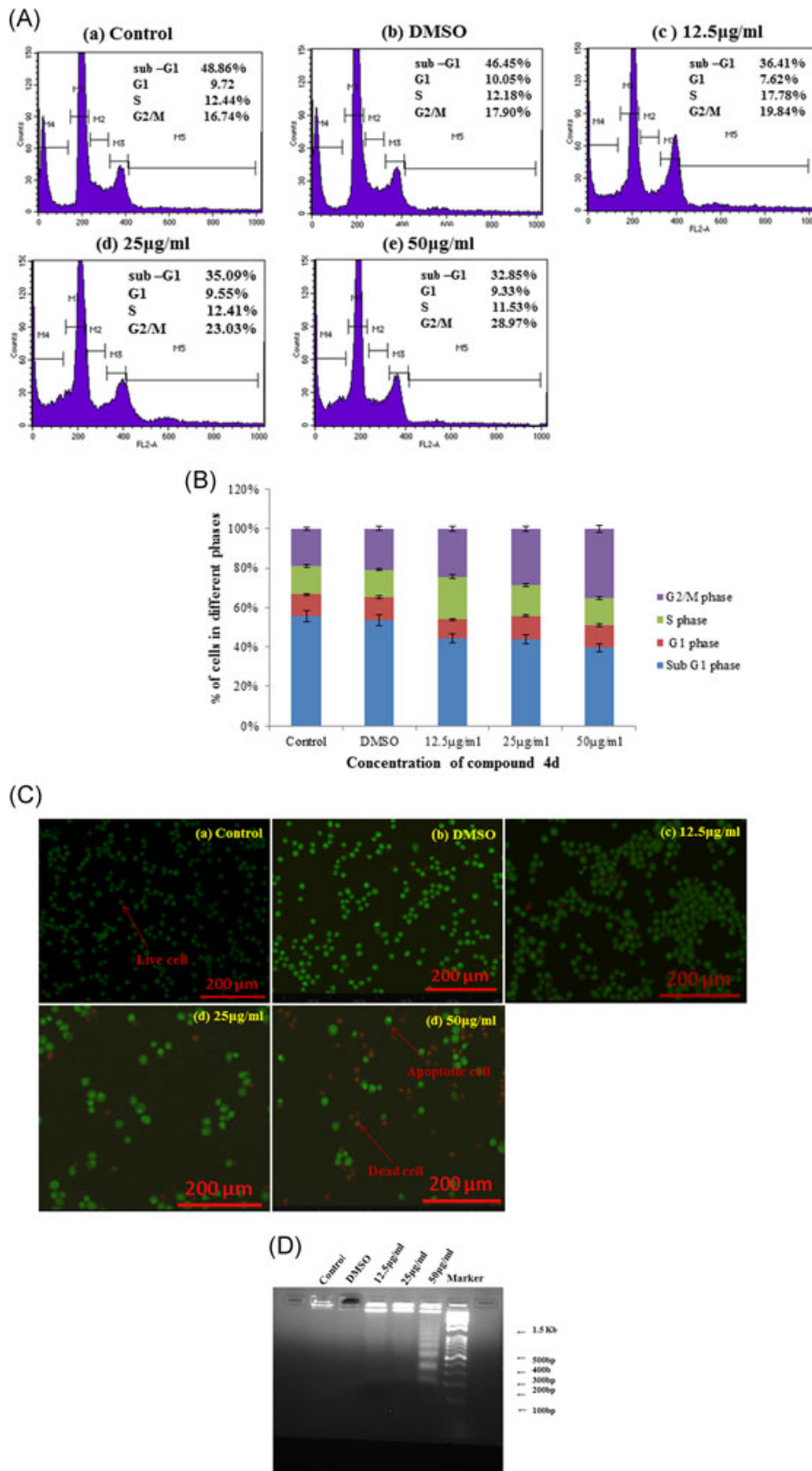


FIGURE 4 A, Cell cycle analysis of HeLa cells treated with different concentrations of **4d** for 24 hours. The cell cycle distribution was performed by using propidium iodide staining and analyzed by flow cytometry BD FACS CALIBUR 4C. B, Histogram of cell cycle distribution (%) in HeLa cells treated with different concentrations of **4d** for 24 hours. Values are expressed as mean \pm SD of three different experiments with $P < 0.05$. C, Compound **4d** induced apoptosis in HeLa cells after 24 hours posttreatment as detected by EtBr/AO staining assay. Green, orange, and red fluorescence indicates live, apoptotic, and dead cells, respectively. Images were captured by fluorescence microscope (Nikon ECLIPSE TiE) at $\times 10$ magnification. D, Effect of **4d** compound on HeLa cells by DNA ladder assay 24 hours posttreatment: 2% agarose gel showing the cleavage of HeLa cells genomic DNA. AO, acridine orange; EtBr, ethidium bromide; DMSO, dimethyl sulfoxide

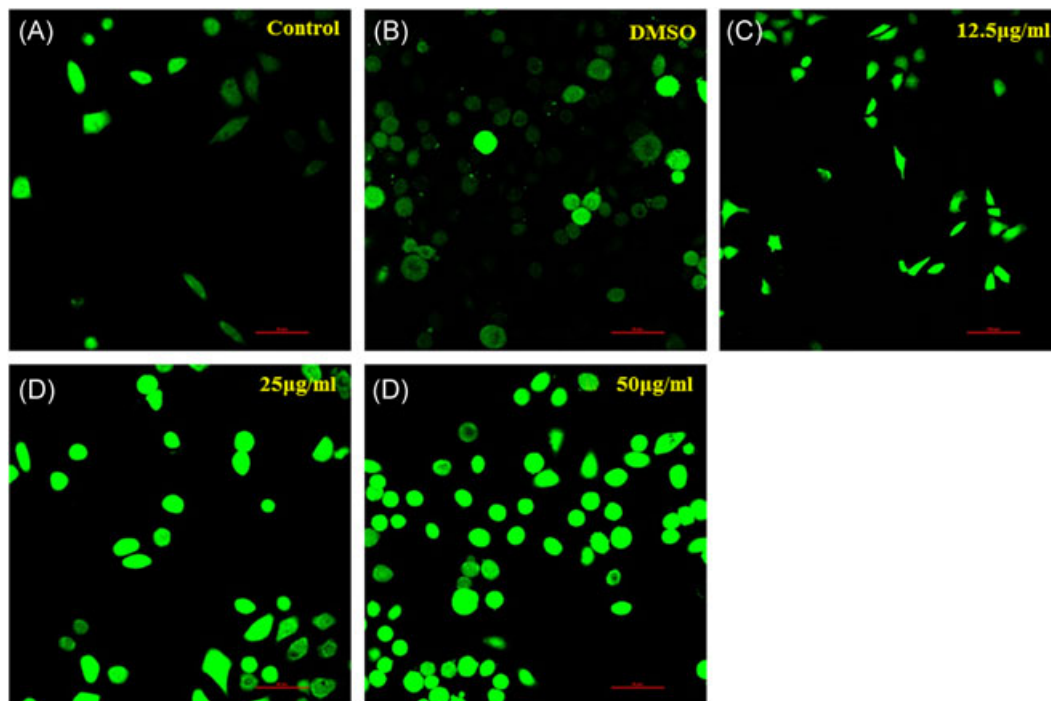


FIGURE 5 Effect of different concentrations of compound **4d** on the ROS production in HeLa cells stained with DCFHDA green indicator after 24 hours treatment. Images were captured by fluorescence microscope (Nikon ECLPSE Ti-E) at $\times 20$ magnification. DCFHDA, dichloro-dihydro-fluorescein diacetate; DMSO, dimethyl sulfoxide; ROS, reactive oxygen species

3.2.6 | Effect of *N*-benzhydryl-4-(5-(4-aminophenyl)-1,3,4-oxadiazol-2-yl)methyl)piperazine (**4d**) on generation of cellular ROS

ROS played an important role in regulation of apoptosis; therefore, to evaluate the ROS produced in treated HeLa cells, DCFHDA a fluorescent probe was used. The intensity of the green fluorescence directly relates to the amount of ROS generated in the cells. HeLa cells on treated with varying concentrations of compound **4d** for 24 hours exhibited considerable intense green fluorescence in contrast to untreated cells (control) which showed weak and diffused fluorescence (Figure 5).

3.2.7 | Effect of *N*-benzhydryl-4-((5-(4-aminophenyl)-1,3,4-oxadiazol-2-yl)methyl)piperazine (**4d**) on mitochondrial membrane potential ($\Delta\psi_m$)

To evaluate the variations in mitochondrial membrane potential, JC-1 dye was used as it exhibits red fluorescent aggregates and green fluorescent monomers predominantly existing in mitochondria and cytosol, respectively, representing high and low membrane potential. It was observed that treated HeLa cells exhibited intense green

fluorescence whereas untreated cells (control cells) displayed intense red fluorescence in concentration dependent manner signifying loss in membrane potential induced by compound **4d** (Figure 6A). Also, it was observed that decrease in the percentage of mitochondria membrane potential varied from 100% (control) to 70.23%, 51.04%, and 40.79% at 12.5, 25, and 50 $\mu\text{g}/\text{mL}$ concentrations of compound **4d**, respectively (Figure 6B).

3.2.8 | Effect of *N*-benzhydryl-4-((5-(4-aminophenyl)-1,3,4-oxadiazol-2-yl)methyl)piperazine (**4d**) on release of cyt *C* and activation of caspase-3

The loss of mitochondrial membrane potential leads to release of cyt *C* from mitochondria to cytosol, which is considered to be a crucial process occurring before the initiation of apoptosis. Considering this, we observed changes in the expression of cytosolic cyt *C* in treated HeLa cells. The results of Western blot analysis showed an increase in the expression of cyt *C* in concentration dependent treatment with compound **4d** (Figure 7A). Additionally, it is evident that cyt *C* activates caspases on being translocated into cytosol from mitochondria leading to apoptosis. It was also observed that compound **4d** upregulated the expression of caspase thus increasing its activation (Figure 7A). The increase in the protein fold

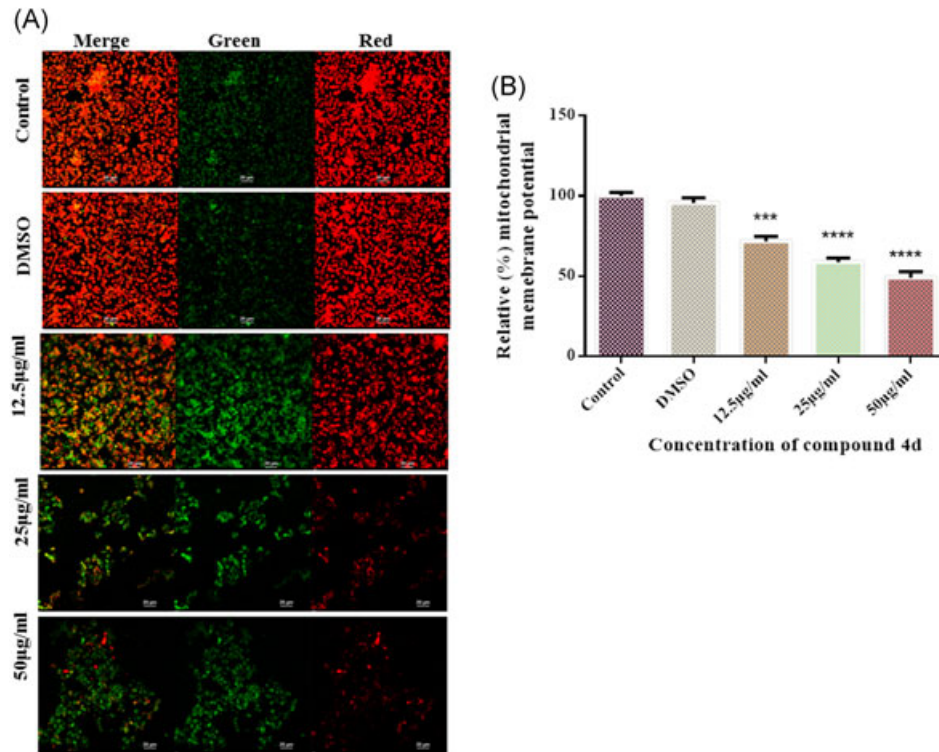


FIGURE 6 A, Effect of different concentrations of compound **4d** on mitochondrial membrane potential in HeLa cells stained with JC-1. Images were captured using live imaging microscope (Nikon ECLIPSE Ti) at $\times 20$ magnification. B, Histogram of relative percentage of mitochondrial membrane potential (in HeLa cells treated with compound **4d** with 12.5, 25, and 50 $\mu\text{g}/\text{mL}$ for 24 hours). Values are expressed as mean \pm SD of triplicates. **** $P < 0.0001$ and *** $P < 0.001$, significant vs control. DMSO, dimethyl sulfoxide

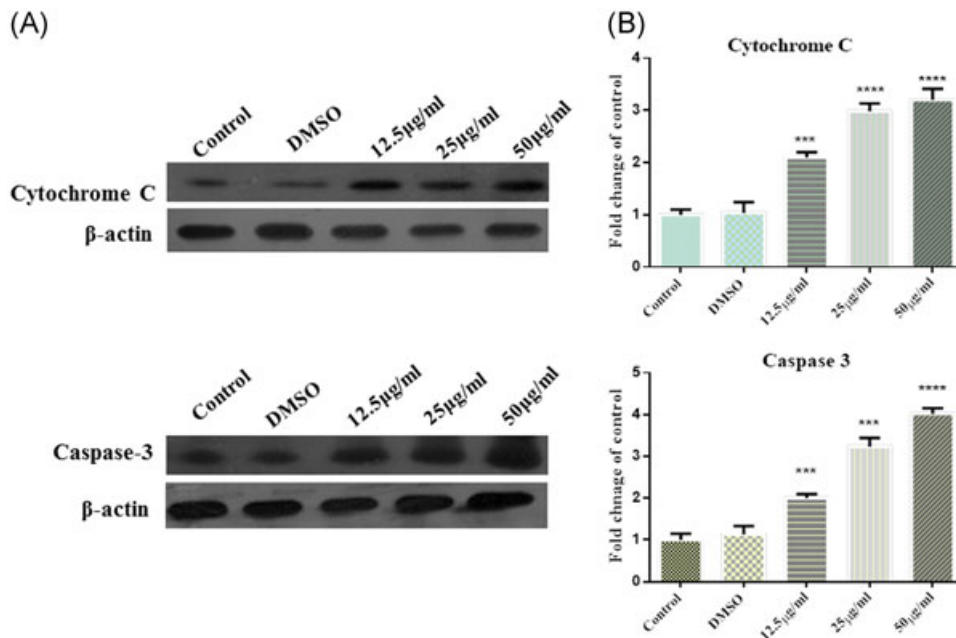


FIGURE 7 A, HeLa cells exposed to different concentrations of **4d** for 24 hours then total protein and cytosolic protein extract were analyzed by Western blot analysis for Cytochrome C in cytosolic protein fraction and caspase-3 in total cells protein extract. B, Bar graph representing the fold changes in the protein expression compared to loading control β -actin. Data expressed as mean \pm SEM of triplicates. *** $P < 0.001$ and **** $P < 0.0001$ significant vs control. DMSO, dimethyl sulfoxide

with respect to control was evaluated using Image J software (Figure 7B).

4 | DISCUSSION

The MTT viability assay showed that the antiproliferation of HeLa cancer cells is due to the variations present within the structural framework of the synthesized compounds. The effect of the phenyl substituted ring attached with 1,3,4-oxadiazoles at C-5 atom was crucial for analyzing the structure and activity relationship (Scheme 1). The compound with unsubstituted phenyl ring (**4a**) was found to be less active and effective in comparison with the compounds with substituted phenyl ring (**4b-4h**). The presence of strong electron donating group like $-NH_2$ (**4d**) and strong electron withdrawing group like $-NO_2$ (4 hours) at para position considerably increased the inhibitory effects on HeLa cells in comparison with weak electron donating groups (**4e, 4f**) or withdrawing groups (**4b, 4c**). In general, substitution at para position enhances the anticancer activity of synthesized compounds.

Recently studies had highlighted the anticancer potential of *N*-benzhydrylpiperazine and 1,3,4-oxadiazoles. Gurdal et al¹⁸ had reported the cytotoxicity of *N*-benzhydrylpiper-

azine derivatives against HUH-7, MCF-7 and HCT-116 cancer cell lines, however, the underlying cellular mechanism remained unexplored, likewise Zheng et al³⁵ had reported that oxadiazole derivatives induced apoptosis in MGC-803 cells. Lately, Zhao et al³⁶ showed that 1,3,4-oxadiazole derivatives induced apoptosis in MDA-MB-231 but the mechanism remained unclear. We have investigated the possible mechanism involved in the induction of apoptosis by compound **4d** (*N*-benzhydryl-4-((5-(4-aminophenyl)-1,3,4-oxadiazol-2-yl)methyl)piperazine) in HeLa cells. Our study had provided the new insight for the mechanism of action of compound **4d** against HeLa cancer cells.

The current study reflects the cytotoxicity of compound **4d** which induced cell death by causing characteristic cell morphological changes (Figure 2A) and reducing the colonies formation of cancer cells (Figure 2B)³⁷ in a concentration dependent treatment. Cell cycle regulates the growth of cells, therefore, various chemotherapeutics were developed targeting cell cycle arrest at precise checkpoint to hinder proliferation of cells.³⁸ Compound **4d** initiated apoptosis by arresting G2/M cell cycle phase with simultaneous decrease in the proportions of cells in sub-G1 phase (Figure 4A and 4B). After evaluating cell cycle arrest at G2/M phase, nuclear

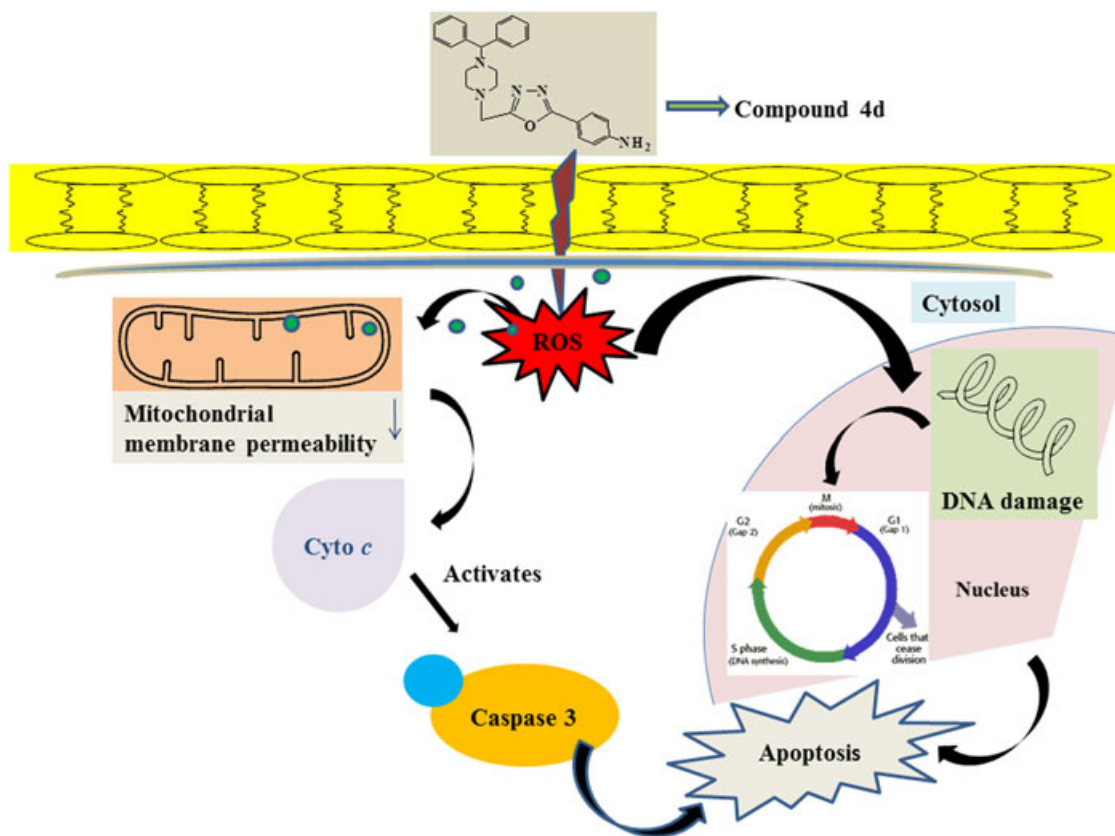


FIGURE 8 Proposed mechanism for induction of apoptosis by *N*-Benzhydryl-4-((5-(4-aminophenyl)-1,3,4-oxadiazol-2-yl)methyl)piperazine (**4d**) in human cervical cancer cell lines (HeLa)

morphology of HeLa cancer cells was studied using AO/EtBr staining assay. AO/EtBr stained HeLa cells observed under fluorescence microscopy showed irregular distribution of chromatin and destructive fragmentation signifying apoptosis been induced by compound **4d**³⁹ (Figure 4C). It was also shown that compound **4d** degraded DNA by forming ladder (Figure 4D) there are many studies been reported which supports that inter-nucleosomal DNA fragmentation is a strong indicator for occurrence of apoptosis.⁴⁰

Some anticancer agents induce apoptosis by increasing an oxidative stress in cell.⁴¹ Increased oxidative stress increased ROS generation which in turn activates the mitochondrial-related apoptotic signals by oxidizing mitochondrial membrane proteins leading to loss of mitochondrial membrane potential.⁴² Our investigations had demonstrated that higher concentration of compound **4d** ($2 \times IC_{50}$) remarkably enhanced the intracellular ROS production (Figure 5) and also decreased the mitochondrial membrane potential (Figure 6A and 6B). We had also studied that the compound **4d** upregulated the expression of cyt C which leads to release of cyt C in cytosol as evident from mitochondrial dysfunction. Released cyt C further activates executioners of caspases.⁴¹ Activated caspase-3 causes cell death by cleaving various death substrates at higher concentration of compound **4d**, that is, at 50 $\mu\text{g}/\text{mL}$ (Figure 7A and 7B).

Besides cell death, the compound **4d** also potentially inhibited the migration of HeLa cells both in concentration and time dependent treatment. 1,3,4-oxadiazole derivatives were shown to inhibit the migration and induced apoptosis in MCF-7 cells in our previous investigation⁴³ thus signifying that the migration is possibly inhibited by compound **4d** due to presence of oxadiazole ring (Figure 3A and 3B).

The investigations were found to be consistent with the proposed hypothesis of apoptosis induction by piperazine-oxadiazole conjugates in treated HeLa cells through generation of oxidative stress-mediated mitochondrial intrinsic pathway (Figure 8).

5 | CONCLUSION

Our investigations showed that compound **4d** (*N*-benzhydryl-4-((5-(4-aminophenyl)-1,3,4-oxadiazol-2-yl)methyl)piperazine), displayed significant anticancer activities by suppressing proliferation of HeLa cells via apoptosis induction. Our findings also provided new insights into mechanisms for compound **4d** induced apoptosis in HeLa cells which may occur through intrinsic mitochondrial pathway. However, investigating other possible pathways

involved in anticancer potential of compound **4d** and in vivo studies still need to be explored.

ACKNOWLEDGMENT

This study was supported by grants UGC (grant nos 41-236/2012 (SR) and 13/07/2012).

CONFLICTS OF INTEREST

The authors declare that there are no conflicts of interest.

ORCID

Rashmin khanam  <http://orcid.org/0000-0003-3618-3112>

REFERENCES

- Small W, Bacon MA, Bajaj A, et al. Cervical cancer: A global health crisis. *Cancer*. 2017;123:2404-2412.
- Ovais M, Khalil AT, Raza A, et al. Green synthesis of silver nanoparticles via plant extracts: beginning a new era in cancer theranostics. *Nanomedicine*. 2016;12:3157-3177.
- Barabadi H, Alizadeh A, Ovais M, Ahmadi A, Shinwari ZK, Saravanan M. Efficacy of green nanoparticles against cancerous and normal cell lines: a systematic review and meta-analysis. *IET Nanobiotechnol*. 2017;12:377-391.
- World Health Organization. GLOBOCAN2012: estimated cancer incidence, mortality and prevalence worldwide in 2012. International Agency for Research on Cancer Population Fact Sheets, Iran, Republic of Islamic; 2014.
- Pidugu VR, Yarla NS, Bishayee A, Kalle AM, Satya AK. Novel histone deacetylase 8-selective inhibitor 1, 3, 4-oxadiazole-alanine hybrid induces apoptosis in breast cancer cells. *Apoptosis*. 2017;22:1394-1403.
- Thongsom S, Suginta W, Lee KJ, Choe H, Talabnin C. Piperlongumine induces G2/M phase arrest and apoptosis in cholangiocarcinoma cells through the ROS-JNK-ERK signaling pathway. *Apoptosis*. 2017;22:1473-1484.
- Subbaiya R, Saravanan M, Priya AR, et al. Biomimetic synthesis of silver nanoparticles from *Streptomyces atrovirens* and their potential anticancer activity against human breast cancer cells. *IET Nanobiotechnol*. 2017;11:965-972.
- Hejazi II, Khanam R, Mehdi SH, et al. New insights into the antioxidant and apoptotic potential of *Glycyrrhiza glabra* L. during hydrogen peroxide mediated oxidative stress: an in vitro and in silico evaluation. *Biomed Pharmacother*. 2017;94:265-279.
- Hejazi II, Khanam R, Mehdi SH, et al. Antioxidative and anti-proliferative potential of *Curculigo orchoides* Gaertn in oxidative stress induced cytotoxicity: in vitro, ex vivo and in silico studies. *Food Chem Toxicol*. 2018;115:244-259.
- Alshatwi AA, Periasamy VS, Athinarayanan J, Elango R. Synergistic anticancer activity of dietary tea polyphenols and bleomycin hydrochloride in human cervical cancer cell: caspase-dependent and independent apoptotic pathways. *Chem Biol Interact*. 2016;247:1-10.

11. Wang L, Wang T, Yang B, Chen Z, Yang H. Design, synthesis, and anti-allergic activities of novel (R)-1-[(4-chlorophenyl) phenyl methyl] piperazine derivatives. *Med Chem Res*. 2012;21:124-132.
12. Zamponi GW, Feng Z-P, Zhang L, et al. Scaffold-based design and synthesis of potent N-type calcium channel blockers. *Bioorg Med Chem Lett*. 2009;19:6467-6472.
13. Punkvang A, Saparpakorn P, Hannongbua S, Wolschann P, Berner H, Pungpo P. Insight into crucial inhibitor-enzyme interaction of arylamides as novel direct inhibitors of the enoyl ACP reductase (InhA) from *Mycobacterium tuberculosis*: computer-aided molecular design. *Monatshefte für Chemie (Chem Monthly)*. 2010;141:1029-1041.
14. Senthilkumar P, Dinakaran M, Banerjee D, et al. Synthesis and antimycobacterial evaluation of newer 1-cyclopropyl-1,4-dihydro-6-fluoro-7-(substituted secondary amino)-8-methoxy-5-(sub)-4-oxoquinoline-3-carboxylic acids. *Bioorg Med Chem*. 2008;16:2558-2569.
15. Srinivasan S, Gupta S, Marwah R. Synthesis, characterization and in vitro biological studies of novel N-aryl piperazinyl fluoroquinolones. *Res J Pharm Biol Chem Sci*. 2010;1:208-218.
16. Chern J-H, Shia K-S, Hsu T-A, et al. Design, synthesis, and structure-activity relationships of pyrazolo [3, 4-d] pyrimidines: a novel class of potent enterovirus inhibitors. *Bioorg Med Chem Lett*. 2004;14:2519-2525.
17. Curreli F, Zhang H, Zhang X, et al. Virtual screening based identification of novel small-molecule inhibitors targeted to the HIV-1 capsid. *Bioorg Med Chem*. 2011;19:77-90.
18. Gurdal E, Yarim M, Durmaz I, Cetin-Atalay R. Cytotoxic activities of some novel benzhydrylpiperazine derivatives. *Drug Res*. 2013;34:121-128.
19. Kumar CSA, Prasad SBB, Vinaya K, et al. Synthesis and in vitro antiproliferative activity of novel 1-benzhydrylpiperazine derivatives against human cancer cell lines. *Eur J Med Chem*. 2009;44:1223-1229.
20. Yarim M, Koksall M, Durmaz I, Atalay R. Cancer cell cytotoxicities of 1-(4-substitutedbenzoyl)-4-(4-chlorobenzhydryl) piperazine derivatives. *Int J Mol Sci*. 2012;13:8071-8085.
21. Sun J, Ren S-Z, Lu X-Y, et al. Discovery of a series of 1, 3, 4-oxadiazole-2 (3H)-thione derivatives containing piperazine skeleton as potential FAK inhibitors. *Bioorg Med Chem*. 2017;25:2593-2600.
22. Guo F-J, Sun J, Gao L-L, et al. Discovery of phenylpiperazine derivatives as IGF-1R inhibitor with potent antiproliferative properties in vitro. *Bioorg Med Chem Lett*. 2015;25:1067-1071.
23. Dias da Silva D, Silva MJ, Moreira P, et al. In vitro hepatotoxicity of 'Legal X': the combination of 1-benzylpiperazine (BZP) and 1-(m-trifluoromethylphenyl) piperazine (TFMPP) triggers oxidative stress, mitochondrial impairment and apoptosis. *Arch Toxicol*. 2017;91:1413-1430.
24. Zhang F, Wang XL, Shi J, et al. Synthesis, molecular modeling and biological evaluation of N-benzylidene-2-((5-(pyridin-4-yl)-1,3,4-oxadiazol-2-yl)thio)acetohydrazide derivatives as potential anticancer agents. *Bioorg Med Chem*. 2014;22:468-477.
25. Valente S, Trisciuglio D, De Luca T, et al. 1,3,4-Oxadiazole-containing histone deacetylase inhibitors: anticancer activities in cancer cells. *J Med Chem*. 2014;57:6259-6265.
26. Du QR, Li DD, Pi YZ, et al. Novel 1,3,4-oxadiazole thioether derivatives targeting thymidylate synthase as dual anticancer/antimicrobial agents. *Bioorg Med Chem*. 2013; 21:2286-2297.
27. Gunosewoyo H, Midzak A, Gaisina IN, et al. Characterization of maleimide-based glycogen synthase kinase-3 (GSK-3) inhibitors as stimulators of steroidogenesis. *J Med Chem*. 2013;56:5115-5129.
28. Cai Z, Wei D, Borzilleri RM, et al. Synthesis, SAR, and evaluation of 4-[2,4-difluoro-5-(cyclopropylcarbamoyl)phenylamino]pyrrolo[2,1-f][1,2,4]triazine-based VEGFR-2 kinase inhibitors. *Bioorg Med Chem Lett*. 2008;18:1354-1358.
29. Yarden Y. The EGFR family and its ligands in human cancer. signalling mechanisms and therapeutic opportunities. *Eur J Cancer*. 2001;37(suppl 4):S3-S8.
30. Chen H, Li Z, Han Y. Synthesis and fungicidal activity against *Rhizoctonia solani* of 2-alkyl (alkylthio)-5-pyrazolyl-1,3,4-oxadiazoles (Thiadiazoles). *J Agric Food Chem*. 2000;48:5312-5315.
31. Kumar R, Tiku AB. Galangin induces cell death by modulating the expression of glyoxalase-1 and Nrf-2 in HeLa cells. *Chem Biol Interact*. 2018;279:1-9.
32. Khanam R, Kumar R, Hejazi II, et al. Piperazine clubbed with 2-azetidinone derivatives suppresses proliferation, migration and induces apoptosis in human cervical cancer HeLa cells through oxidative stress mediated intrinsic mitochondrial pathway. *Apoptosis*. 2018;23:1-19.
33. Wani MY, Ahmad A, Shiekh RA, Al-Ghamdi KJ, Sobral AJ. Imidazole clubbed 1, 3, 4-oxadiazole derivatives as potential antifungal agents. *Bioorg Med Chem*. 2015;23:4172-4180.
34. Morris GM, Goodsell DS, Halliday RS, et al. Automated docking using a Lamarckian genetic algorithm and an empirical binding free energy function. *J Computat Chem*. 1998;19:1639-1662.
35. Zheng Q-Z, Zhang X-M, Xu Y, Cheng K, Jiao Q-C, Zhu H-L. Synthesis, biological evaluation, and molecular docking studies of 2-chloropyridine derivatives possessing 1, 3, 4-oxadiazole moiety as potential antitumor agents. *Bioorg Med Chem*. 2010;18:7836-7841.
36. Zhao J-J, Wang X-F, Li B-L, et al. Synthesis and in vitro antiproliferative evaluation of novel nonsymmetrical disulfides bearing 1, 3, 4-oxadiazole moiety. *Bioorg Med Chem Lett*. 2016;26:4414-4416.
37. Xu X-m, Chen Y, Jiang P, Dong C-z, Wang Q. Apoptosis of human Burkitt's lymphoma cells induced by 2-N, N-diethylaminocarbonyloxymethyl-1-diphenylmethyl-4-(3, 4, 5-trimethoxybenzoyl) piperazine hydrochloride (PMS-1077). *Arch Pharm Res*. 2009;32: 1727-1736.
38. Wang XD, Sun YY, Zhao C, Qu FZ, Zhao YQ. 12-Chloroacetyl-PPD, a novel dammarane derivative, shows anti-cancer activity via delay the progression of cell cycle G2/M phase and reactive oxygen species-mediate cell apoptosis. *Eur J Pharmacol*. 2017;798:49-56.
39. Aarts M, Sharpe R, Garcia-Murillas I, et al. Forced mitotic entry of S-phase cells as a therapeutic strategy induced by inhibition of WEE1. *Cancer Discov*. 2012;2:524-539.
40. Tan B-J, Chiu GNC. Role of oxidative stress, endoplasmic reticulum stress and ERK activation in triptolide-induced apoptosis. *Int J Oncol*. 2013;42:1605-1612.
41. Simon H-U, Haj-Yehia A, Levi-Schaffer F. Role of reactive oxygen species (ROS) in apoptosis induction. *Apoptosis*. 2000;5:415-418.
42. Shyam H, Singh N, Kaushik S, Sharma R, Balapure AK. Centchroman induces redox-dependent apoptosis and cell-cycle arrest in human endometrial cancer cells. *Apoptosis*. 2017;22:570-584.

43. Khanam R, Ahmad K, Hejazi II, et al. Inhibitory growth evaluation and apoptosis induction in MCF-7 cancer cells by new 5-aryl-2-butylthio-1, 3, 4-oxadiazole derivatives. *Cancer Chemother Pharmacol*. 2017;80:1027-1042.

SUPPORTING INFORMATION

Additional supporting information may be found online in the Supporting Information section at the end of the article.

How to cite this article: Khanam R, Kumar R, Hejazi II, et al. New *N*-benzhydrylpiperazine/1,3,4-oxadiazoles conjugates inhibit the proliferation, migration, and induce apoptosis in HeLa cancer cells via oxidative stress-mediated mitochondrial pathway. *J Cell Biochem*. 2018;1-16.

<https://doi.org/10.1002/jcb.27472>